THE JOURNAL OF PHYSICAL CHEMISTRY C

Article

Effect of Water Vapor on Electrical Properties of Individual Reduced Graphene Oxide Sheets

Inhwa Jung, Dmitriy Dikin, Sungjin Park, Weiwei Cai, Steven L. Mielke, and Rodney S. Ruoff

J. Phys. Chem. C, **2008**, 112 (51), 20264-20268 • Publication Date (Web): 03 December 2008

Effect of Water Vapor on Electrical Properties of Individual Reduced Graphene Oxide Sheets

Inhwa Jung,[†] Dmitriy Dikin,[‡] Sungjin Park,[†] Weiwei Cai,[†] Steven L. Mielke,[§] and Rodney S. Ruoff*,[†]

Department of Mechanical Engineering, the University of Texas at Austin, Austin, Texas, 78712, Department of Mechanical Engineering, Northwestern University, Evanston, Illinois 60208, Department of Chemistry, University of Minnesota, Minneapolis, Minnesota 55455

Received: August 22, 2008; Revised Manuscript Received: October 20, 2008

The electrical conductivity and gas-sensing characteristics of individual sheets of partially reduced graphene oxide are studied, and the results display a strong dependence on the chosen reduction method. Three reduction procedures are considered here: thermal, chemical, and a combined chemical/thermal approach. Samples treated by chemical/thermal reduction display the highest conductivity whereas thermally reduced samples display the fastest gas-sensing response times. The chemo-resistive response to water vapor adsorption is well fit by a linear driving force model. The conductivity upon exposure to water vapor and measured as a function of the gated electric field displays significant hysteresis. These results illustrate how the chemical structure of graphene oxide may be tailored to optimize specific properties for applications such as field effect devices and gas sensors.

1. Introduction

Carbon nanostructures hold great potential as materials for high-sensitivity gas-sensing applications;[1,2] indeed, the sensitivity of graphene-based sensors can be so high that single-molecule detection is possible.[3] However, methods for obtaining graphene, such as micromechanical exfoliation[4] and epitaxial growth,[5] have critical drawbacks in terms of yield quantity and cost. Graphene oxide, which is an individual layer of oxidized graphite, is advantageous in these respects because it may be obtained by chemical processing.[6] The chemical structure of graphene oxide is not well established, but is believed to include a variety of oxygen functional groups, such as epoxide and hydroxyl groups on the interior of the sheet and carbonyl and carboxyl groups at the edges.[7−10] Due to these oxygenated groups, chemical and opto-electrical characteristics deviate significantly from those of graphene. Thus, the presence of oxygenated groups provides opportunities to tailor the material for specific uses through modification. Presently, modification is aimed at enhancing electrical conductivity, improving dispersability of nanoinclusions in nanocomposites,[11,12] and electronic device applications.[13,14]

As synthesized, graphite oxide typically possesses a carbon-to-oxygen ratio of about 2 and the material is nonconducting and hygroscopic. As the material is reduced and the carbon-to-oxygen ratio increases, portions of the graphitic network are restored, and after percolation is achieved for a given specimen, the conductivity increases and eventually will plateau.[15] Herein we consider three procedures for reducing graphene oxide and study the effects of these approaches on the material properties, in particular, the conductivity and gas-sensing properties. Thermal and chemical (reaction with hydrazine was considered here) reduction methods may be used to treat graphene oxide and a third regime employing sequential chemical and thermal treatments was also considered.

Much work remains before a detailed understanding of the chemical structure of graphite oxide and reduced graphene oxide sheets is achieved. The present effort employs simple reduction schemes that permit modification of entire sheets. Ultimately, techniques such as dip pen nanolithography may permit finely controlled reduction and thus allow nanoengineering of individual sheets. Furthermore, the degree to which the chemical properties of the reduced graphene oxide sheets vary with the reduction protocol needs to be carefully explored. Thus, it is of a great interest to study the effects of reduction methods on the electrical properties and chemical sensitivity, which will provide crucial information about the prospects for using these materials as sensors. This study is a first step toward the goal of chemically functionalizing such materials for specific gas-sensing applications.

2. Experimental Details

In this work, graphene oxide-based field effect devices were made by depositing, identifying, and studying an individual graphene oxide sheet on a silicon-dioxide-grown highly doped silicon substrate. Conductivity and conductivity changes as a function of an applied electric field were determined by a four-probe configuration. Graphene oxide samples were reduced by heating in vacuum or by exposure to hydrazine gas. $I-V$ characteristics at each reduction step and the final saturated conductivities were measured. The electrical responses of graphene oxide upon exposure to water vapor were measured for samples obtained by different reduction schemes. The change of the electric field effect upon exposure to water vapor is also investigated.

Samples were prepared as follows. A silicon dioxide layer of a desired thickness (300 ± 10 nm) was grown on a highly doped *p*-type silicon wafer, and then alignment marks were patterned on these substrates. Individual graphene oxide sheets

* Corresponding author: tel (512) 471-4691; e-mail r.ruoff@mail.utexas.edu.
[†] University of Texas at Austin.
[‡] Northwestern University.
[§] University of Minnesota.

10.1021/jp807525d CCC: $40.75
Published on Web 12/03/2008

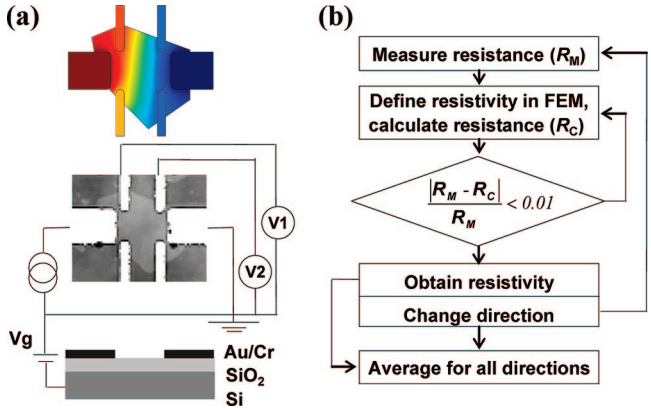

Figure 1. Device schematics and resistivity determination procedure. (a) Four-probe configuration for measuring conductivity and gate dependence with a confocal microscope image (at 543 nm wavelength) of the sample. The upper panel shows an example of the calculated distribution of electric potential for the indicated combination of current and voltage probes; red and blue coloring indicate regions of higher and lower potential, respectively. (b) Schematic of the procedure for determining the sample resistivity (conductivity) based on measured values and FEM fitting.

deposited on the substrate were identified by confocal microscopy.[16] Alignment marks were used to find the same sheet with a confocal microscope and atomic force microscopy (AFM). On the basis of optical images, thin metal electrodes (5-nm Cr followed by 50-nm Au) were deposited on naturally shaped sheets of graphene oxide. Three types of samples were made, each with a different number of electrodes (4, 6, or 12); a 6-electrode sample is shown in Figure 1a. Thermal reduction and electrical measurements of graphene oxide sheets were performed simultaneously inside a vacuum chamber of a scanning electron microscope (Nova NanoSEM600, FEI Co.). The base pressure of the chamber was about 10^{-5} Torr, but water vapor could be introduced following the standard procedure of variable pressure SEM. A vacuum-compatible sample holder with an integrated heater and thermometer was custom-built to facilitate electrical-property measurements within the chamber. The chemical treatment was performed by exposing the sample to hydrazine vapor (evolving from hydrazine monohydrate, 98%, Aldrich) at 70 °C for 24 h. (For detailed sample preparation and experimental procedures, see Supporting Information.)

In order to get the best estimate of the sample's conductivity, we used all possible combinations of current and voltage probes to account for the sample shape and the electrode positions with respect to the sample edges. This imperfect van der Pauw configuration[17] did not permit a simple analytical calculation, so instead we applied a finite elements method (FEM) using the multiphysics modeling software COMSOL, which we have already used for our high-resistive composite samples.[11,18] (For further details of the numerical modeling, see Supporting Information.) An example of the calculated distribution of the electric potential is shown in Figure 1a. The graphene oxide sheet's resistance was determined by dividing the potential difference between two electrodes by the total current flow, with the assumption of a 1-nm sample thickness. The procedure for determining sample resistivity is sketched in Figure 1b. Based on an assumed value of resistivity for a particular combination of electrodes, the sample resistance was calculated and compared with the measured value. The estimated material resistivity (conductivity) was then refined until the difference between the measured and calculated values converged to within 1%. The measurements and calculations were repeated for different combinations of current and voltage probes, and the conductivity value for each sample was taken as the average value of all calculated directions.

3. Results and Discussion

The maximum attainable conductivities of isolated graphene oxide sheets from several different reduction routes are compared in Figure 2a. As shown, the conductivities of five thermally reduced samples ranged from 33 to 85 $S \cdot m^{-1}$. The conductivity of the chemically treated material is comparable to that of the thermally treated samples when the dispersion of collected data is considered, but is greatly increased by a subsequent thermal treatment. During thermal reduction of graphene oxide sheets, CO, CO_2, and water are formed.[19] Thermal reduction of graphite oxide powder, which presumably proceeds similarly to that of isolated graphene oxide sheets, has been studied[7,9,20−22] and the CO-to-CO_2 ratio was found to be dependent on experimental conditions. The chemical mechanisms involved in the thermal reduction are not well characterized, but CO is a strong reducing agent, so it is possible that much if not all of the CO_2 production occurs via multistep processes. (Oxidized graphene sheets are a common system model used in the field of combustion chemistry to study char formation, and mechanisms for the readsorption of CO onto highly oxidized surfaces that eventually produce CO_2 have been previously reported.[23]) No significant decrease in the sample dimensions was observed during thermal reduction, so the carbon loss that occurs during the thermal reduction must be widely distributed throughout the sheet and consequently a significant number of vacancies and/or small holes are likely to exist. These defects may serve as binding sites for chemisorption.[24] In contrast, hydrazine reduction is believed to remove the oxygen functional groups without removing carbon,[25,26] so the sheet remains largely intact. Although the hydrazine treatment greatly reduces the degree of functionalization as compared to untreated graphene oxide, it also introduces a significant amount of nitrogen-containing functional groups to the sheet.[26,27] Thus, the binding energies of various adsorbates may be quite different for chemically reduced materials compared to those for thermally reduced materials.

As the graphene oxide sheets are reduced, unfunctionalized graphitic regions form and eventually percolation passes develop, allowing a degree of conductivity to be restored.[15] A number of different factors affect the formation of such regions. When a pristine graphene sheet is functionalized, the bonding at the attachment site is altered from sp^2 to sp^3 character and this leads to a puckering of the sheet. Such distortions are energetically unfavorable; thus, clusters of chemical attachments are more stable than several isolated attachments. This energetic effect may be important in the context of reduction for two reasons. First, we might expect that isolated functional groups will be more reactive than those that are in regions of high functionalization and this may lead to a tendency for patches of graphitic character to form as isolated attachments are preferentially removed. Second, if the functional groups are capable of migrating from one location to another along the sheet, this energetic effect will lead to islands of high- and low-density functionalization developing as a sample is annealed. The barrier for epoxide migration has been estimated by density functional theory calculations[28] to be only about 0.9 eV, so the positions of these groups may be partially reordered. Hydroxyl groups bond strongly to a graphene sheet, so the positions of these groups might be expected to be quite stable; however, Paci et al.[29] have observed hydroxyl and epoxide groups

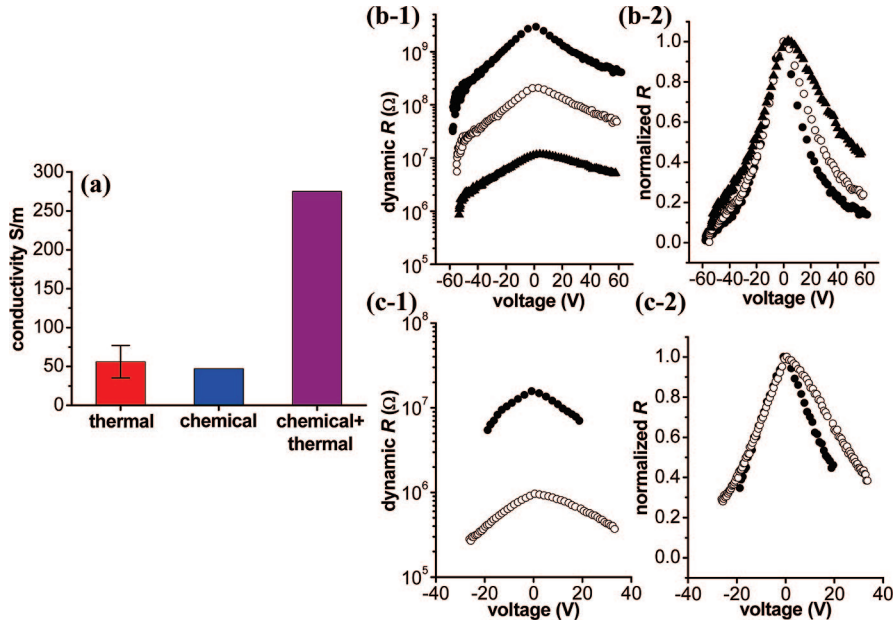

Figure 2. Conductivity value and nonlinearity of $I-V$ characteristics of reduced graphene oxide. (a) Conductivity of single sheets of graphene oxide reduced by three different reduction methods: red, thermal reduction (error bars denote 1 standard deviation); blue, chemical reduction (exposed to air for 1 day and measured in ambient conditions); purple, combined chemical/thermal reduction. (b-1) Resistance of thermally treated sample at three different stages of reduction: (●, upper curve) slightly reduced material, (▲, lower curve) "fully" reduced material, and (○, middle curve) intermediate degree of reduction. (b-2) Normalized dynamic resistance. (c-1) Resistance of (●) hydrazine-treated and (○) hydrazine/thermally treated sample. (c-2) Normalized dynamic resistance.

swapping locations (via a hydrogen transfer step) during high-temperature molecular dynamics simulations.

Judging from previous X-ray photoelectron spectroscopy (XPS) measurements,[25,26] the hydrazine treatment leads to roughly comparable reductions in oxygen functionalization as compared to thermal treatment without the carbon loss and associated defect introduction, but the conductivity restoration is not significantly different from that for the thermally treated samples. Presumably this is because the remaining functional groups are more evenly distributed. An additional thermal treatment leads to a further reduction in the degree of functionalization and possibly some redistribution of what remains. Thus, the chemically and thermally treated sample exhibits a dramatically higher conductivity than that of the other samples. These trends have also recently been noted by Becerril et al.[25]

$I-V$ characteristics were measured at several stages of a thermal reduction, and calculated $R = \mathrm{d}V/\mathrm{d}I$ versus V dependences are shown in Figure 2b,c. As one can see in Figure 2b-1, significant decreases in resistance are measured after each thermal treatment. In all cases the resistance is highest at a voltage close to zero, which is known as the Dirac point in pristine graphene. When the $R(V)$ curves for three stages of reduction are compared by normalization of the dynamic resistance, it is easy to see that a decrease in nonlinear behavior occurs as the samples are more thoroughly reduced. The chemically and thermally treated sample displays the most-linear R versus V behavior.

In an attempt to understand the kinetics of the reduction process, a graphene oxide sample that had undergone a prior thermal reduction to render it slightly conductive ($\sim 10^{11}$ Ω) was further reduced with a programmed temperature profile. When the electrical resistance of the material is plotted in logarithmic scale with the temperature profile (Figure 3a), the magnitude of the slope of the resistance reduction increases with increasing temperature. When the logarithmic values of these slopes are plotted versus the inverse of temperature (Figure 3b), the relationship shows a linear dependence at the higher $1/T$ range but deviates from linearity at lower values ($T \geq 175$ °C). The linear dependence is analogous to Arrhenius behavior, which suggests that the reduction process can be envisioned as a kinetic process controlled by a single dominant activation step. Further analyses of this behavior, including elemental analysis (XPS) and temperature-programmed desorption (TPD), are underway and will be presented elsewhere.

The chemoresistive responses of reduced graphene oxide sheets upon exposure to water vapor of specified pressure were measured and compared. Figure 4a-1 shows the resistance responses of a thermally reduced sample upon exposure to water vapor at different pressures (0.1, 0.53, 1.0, and 1.5 Torr). The curve shows clear demarcations between each intake; a rapid increase is observed at the moment the gas is introduced, followed by saturation after a short exposure time. For comparison, the same experiment was done on a sample that was chemically and then thermally reduced, and these results are shown in Figure 4b-1. The first segment of these response curves are well fitted by the linear driving force (LDF) model as seen in Figure 4 panels a-2 and b-2. The behavior observed is similar to that observed for the adsorption of gases such as oxygen, nitrogen, carbon dioxide, argon, and krypton on carbon molecular sieves (CMS) and for chemisorption on activated carbon.[30−36] The linear driving force model is expressed as $M_t/M_e = 1 - e^{-kt}$, where k is the rate constant, M_t is the uptake at time t, and M_e is the equilibrium uptake, which are correlated with the change of resistance at time t (ΔR) and the change of resistance at the equilibrium state ($\Delta R'$). By comparing rate constants obtained by fitting each curve (Figures 4a-2 and b-2), it is found that the time response of the resistance of graphene oxide to 0.1 Torr of water vapor for a sample reduced by hydrazine and thermal treatment is about 6 times slower than the response of a sample reduced only thermally. The markedly faster response of the thermally reduced sample can be attributed to two effects: first, the thermally reduced sample is expected

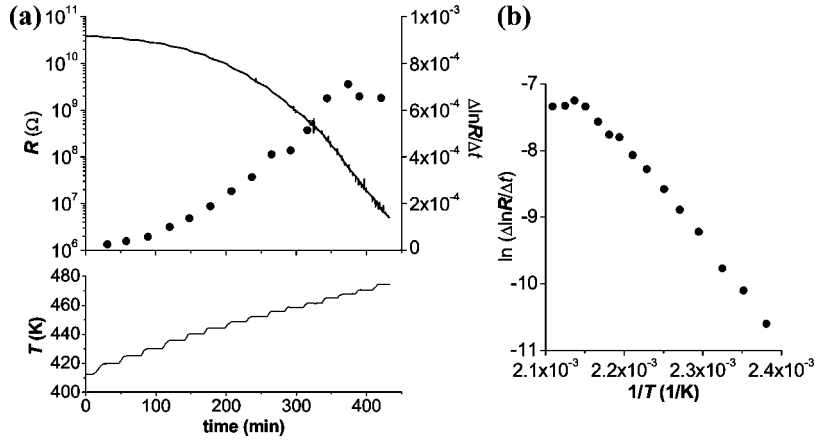

Figure 3. Temperature-programmed thermal reduction of individual graphene oxide sheets. (a, upper panel) Resistance reduction curve (—) and extracted slopes of logarithmic resistance by time (●). (a, lower panel) Temperature profile applied. (b) Relation between the temperature of reduction and logarithm of the extracted slopes.

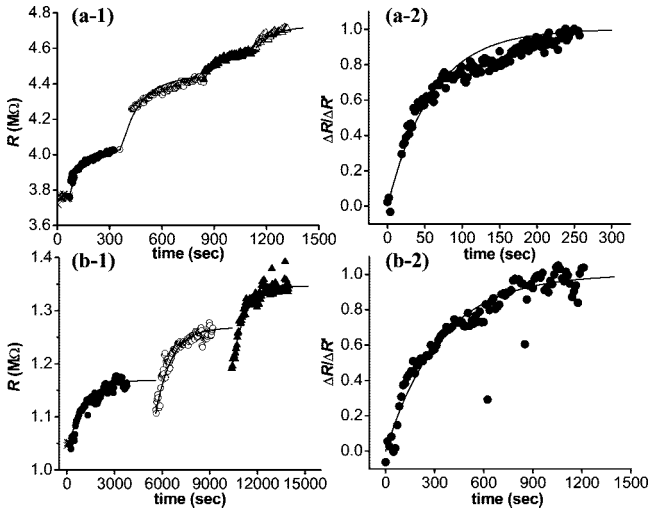

Figure 4. Chemoresistive response to water vapor for individual sheets of reduced graphene oxide (a-1) Resistance of thermally treated sample versus time upon exposure to water vapor: (×) at base pressure (~10^{-5} Torr) before exposure and at (●) 0.1, (○) 0.53, (▲) 1, and (Δ) 1.5 Torr of water vapor. (a-2) Fitted resistance curve obtained with the linear driving force (LDF) model (ΔR is the change of resistance and $\Delta R'$ is the resistance change at the saturated state). (b-1) Resistance of chemically and thermally treated sample versus time upon exposure to water vapor: (×) at base pressure (~10^{-5} Torr) before exposure and at (●) 0.1, (○) 0.53, and (▲) 1.5 Torr of water vapor. (b-2) Fitted resistance curve obtained with the linear driving force model.

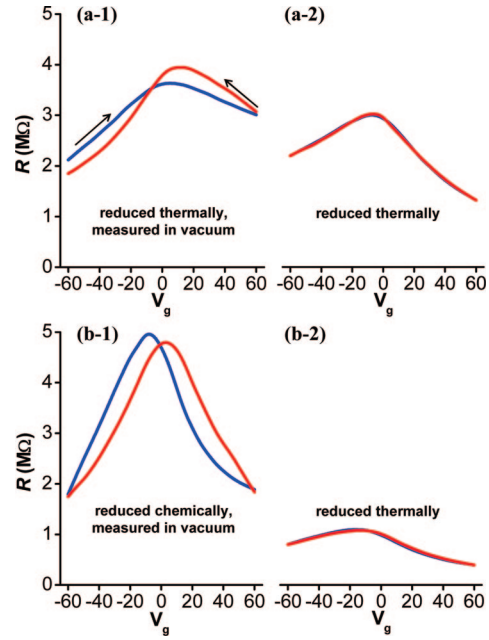

Figure 5. Effect of adsorbed water on individual graphene oxide field effect devices. (a) Effect of thermal treatment: (a-1) sample was thermally treated in vacuum (at $T = 225$ °C, for $t = 120$ min), exposed to air for 1 h, and measured in vacuum; (a-2) the same sample was thermally treated in vacuum ($T = 250$ °C, $t = 60$ min) and measured in vacuum. (b) Effect of chemical and thermal treatments: (b-1) sample was treated by hydrazine, exposed to air for 1 day, and measured in vacuum; (b-2) the same sample was thermally treated in vacuum ($T = 215$ °C, $t = 100$ min) and measured in vacuum. The gate-sweep rate was 0.5 V/s, and the drain-source current was 100 nA for all measurements; gate voltage increased (blue) and decreased (red).

to contain a much larger number of point defects, which serve as strong binding sites, and second, the interaction between water and oxygen functional groups is expected to be stronger than between water and nitrogen functional groups.

The electric field effect was monitored after each reduction step and exposure to gaseous environment. Figure 5a-1 shows the effect of the electric field on the conductivity of a sample that was reduced thermally in vacuum (~10^{-5} Torr), exposed to air for 1 h, and then reinserted into the vacuum chamber for measurement. In general, the behavior follows that reported earlier by Gomez-Navarro et al.[14] A significant hysteresis is evident, which is analogous to the behavior observed for water adsorbed on single-walled carbon nanotube field effect transistors.[37] As discussed by Kim et al.,[37] this is presumably due to charge trapping resulting from water (and various microsolvated contaminants) adsorbed both on the graphene oxide sheet and the underlying substrate. Additional treatment in vacuum causes this hysteresis to disappear as seen in Figure 5a-2. The chemically reduced sample also shows this hysteresis effect (Figure 5b-1), but the resistance change as a function of the gate voltage is more symmetric than for the thermally reduced sample. When an additional thermal treatment is applied to the sample, the conductivity increases by more than a factor of 5 (Figure 5b-2).

4. Concluding Remarks

The electrical conductivity and gas-sensing properties of samples of graphene oxide reduced with three different protocols were studied. The samples that underwent chemical reduction followed by further thermal reduction exhibited the highest conductivity. In contrast, the thermally treated samples displayed

the fastest chemoresistive response upon exposure to water vapor, and we suggest that this is due to a larger number of point defects likely introduced in the thermal process.

The electric field can effectively change the conductivity of single graphene oxide sheets, although this is complicated by a significant hysteresis due to adsorbed water and microsolvated contaminants when measuring in air or water vapor. By analyzing the slope of the resistance reduction curve at different temperatures, but below ~180 °C, it is observed that the rate of the thermal reduction process seems to be dominated by a single kinetic process. The results presented here demonstrate that the chemical functionalization of reduced graphene oxide sheets may be tailored to optimize specific properties, and this suggests that these materials show great promise for use as field effect transistors and chemical sensors.

Acknowledgment. We thank S. Stankovich for synthesis of the graphite oxide used in this study. We gratefully acknowledge support from the DARPA Center on Nanoscale Science and Technology for Integrated Micro/Nano-Electromechanical Transducers (iMINT) (Award HR0011-06-1-0048).

Supporting Information Available: Details of the sample preparation method, experimental procedures, and the numerical modeling are provided. The conductivity of each sample is also provided. This material is available free of charge via the Internet at http://pubs.acs.org.

References and Notes

(1) Kong, J.; Franklin, N. R.; Zhou, C. W.; Chapline, M. G.; Peng, S.; Cho, K. J.; Dai, H. J. *Science* **2000**, *287*, 622.
(2) Collins, P. G.; Bradley, K.; Ishigami, M.; Zettl, A. *Science* **2000**, *287*, 1801.
(3) Schedin, F.; Geim, A. K.; Morozov, S. V.; Hill, E. W.; Blake, P.; Katsnelson, M. I.; Novoselov, K. S. *Nat. Mater.* **2007**, *6*, 652.
(4) Novoselov, K. S.; Geim, A. K.; Morozov, S. V.; Jiang, D.; Zhang, Y.; Dubonos, S. V.; Grigorieva, I. V.; Firsov, A. A. *Science* **2004**, *306*, 666.
(5) Berger, C.; Song, Z. M.; Li, X. B.; Wu, X. S.; Brown, N.; Naud, C.; Mayo, D.; Li, T. B.; Hass, J.; Marchenkov, A. N.; Conrad, E. H.; First, P. N.; de Heer, W. A. *Science* **2006**, *312*, 1191.
(6) Hummers, W.; Offeman, R. *J. Am. Chem. Soc.* **1958**, *80*, 1339.
(7) He, H. Y.; Klinowski, J.; Forster, M.; Lerf, A. *Chem. Phys. Lett.* **1998**, *287*, 53.
(8) He, H. Y.; Riedl, T.; Lerf, A.; Klinowski, J. *J. Phys. Chem.* **1996**, *100*, 19954.
(9) Lerf, A.; He, H. Y.; Forster, M.; Klinowski, J. *J. Phys. Chem. B* **1998**, *102*, 4477.
(10) Lerf, A.; He, H. Y.; Riedl, T.; Forster, M.; Klinowski, J. *Solid State Ionics* **1997**, *101*, 857.
(11) Stankovich, S.; Dikin, D. A.; Dommett, G. H. B.; Kohlhaas, K. M.; Zimney, E. J.; Stach, E. A.; Piner, R. D.; Nguyen, S. T.; Ruoff, R. S. *Nature* **2006**, *442*, 282.
(12) Watcharotone, S.; Dikin, D. A.; Stankovich, S.; Piner, R.; Jung, I.; Dommett, G. H. B.; Evmenenko, G.; Wu, S. E.; Chen, S. F.; Liu, C. P.; Nguyen, S. T.; Ruoff, R. S. *Nano Lett.* **2007**, *7*, 1888.
(13) Gilje, S.; Han, S.; Wang, M.; Wang, K. L.; Kaner, R. B. *Nano Lett.* **2007**, *7*, 3394.
(14) Gomez-Navarro, C.; Weitz, R. T.; Bittner, A. M.; Scolari, M.; Mews, A.; Burghard, M.; Kern, K. *Nano Lett.* **2007**, *7*, 3499.
(15) Jung, I.; Dikin, D. A.; Piner, R.; Ruoff, R. S. *Nano Lett*. **2008**, *8*, 4283−4287.
(16) Jung, I.; Pelton, M.; Piner, R.; Dikin, D. A.; Stankovich, S.; Watcharotone, S.; Hausner, M.; Ruoff, R. S. *Nano Lett.* **2007**, *7*, 3569.
(17) Van der Pauw, L. J. *Philips Res. Rep.* **1958**, *13*, 1.
(18) Zimney, E. J.; Dommett, G. H. B.; Ruoff, R. S.; Dikin, D. A. *Meas. Sci. Technol.* **2007**, *18*, 2067.
(19) Hofmann, U.; Frenzel, A.; Csalan, E. *Liebigs Ann. Chem.* **1934**, *510*, 1.
(20) Matsuo, Y.; Sugie, Y. *Carbon* **1998**, *36*, 301.
(21) Matsuo, Y.; Tahara, K.; Sugie, Y. *Carbon* **1997**, *35*, 113.
(22) Scholz, W.; Boehm, H. P. *Naturwissenschaften* **1964**, *51*, 160.
(23) Sanchez, A.; Mondragon, F. *J. Phys. Chem. C* **2007**, *111*, 612.
(24) Slabaugh, W. H.; Seiler, B. C. *J. Phys. Chem.* **1962**, *66*, 396.
(25) Becerril, H. A.; Mao, J.; Liu, Z.; Stoltenberg, R. M.; Bao, Z.; Chen, Y. *ACS Nano* **2008**, *2*, 463.
(26) Stankovich, S.; Dikin, D. A.; Piner, R. D.; Kohlhaas, K. A.; Kleinhammes, A.; Jia, Y.; Wu, Y.; Nguyen, S. T.; Ruoff, R. S. *Carbon* **2007**, *45*, 1558.
(27) Yang, D.; Velamakanni, A.; Bozoklu, G.; Park, S.; Stoller, M.; Piner, R. D.; Stankovich, S.; Jung, I.; Field, D. A.; Ventrice, C.; Ruoff, R. S. *Carbon* [Online early access]. DOI: 10.1016/j.carbon.2008.09.045.
(28) Li, J.-L.; Kudin, K. N.; McAllister, M. J.; Prud'homme, R. K.; Aksay, I. A.; Car, R. *Phys. Rev. Lett.* **2006**, *96*, 176101.
(29) Paci, J. T.; Belytschko, T.; Schatz, G. C. *J. Phys. Chem. C* **2007**, *111*, 18099.
(30) Chagger, H. K.; Ndaji, F. E.; Sykes, M. L.; Thomas, K. M. *Carbon* **1995**, *33*, 1405.
(31) Fletcher, A. J.; Benham, M. J.; Thomas, K. M. *J. Phys. Chem. B* **2002**, *106*, 7474.
(32) Fletcher, A. J.; Thomas, K. M. *Langmuir* **1999**, *15*, 6908.
(33) Fletcher, A. J.; Thomas, K. M. *Langmuir* **2000**, *16*, 6253.
(34) Harding, A. W.; Foley, N. J.; Norman, P. R.; Francis, D. C.; Thomas, K. M. *Langmuir* **1998**, *14*, 3858.
(35) Reid, C. R.; O'Koye, I. P.; Thomas, K. M. *Langmuir* **1998**, *14*, 2415.
(36) Reid, C. R.; Thomas, K. M. *J. Phys. Chem. B* **2001**, *105*, 10619.
(37) Kim, W.; Javey, A.; Vermesh, O.; Wang, O.; Li, Y. M.; Dai, H. J. *Nano Lett.* **2003**, *3*, 193.

JP807525D